JOURNAL OF PROPULSION AND POWER
Vol. 22, No. 4, July–August 2006

Aerodynamic Performance of Scramjet Inlet Models with a Single Strut

Kouichiro Tani,* Takeshi Kanda,† and Kenji Kudou‡
Japan Aerospace Exploration Agency, Kakuda, Miyagi 981-1525, Japan

A series of three-dimensional sidewall compression-type scramjet inlet models with single struts were tested in a Mach 4 wind tunnel to investigate the influence of a strut between the sidewalls. With the sidewalls having a fixed shape, five struts of the same width but different lengths and wedge angles were mounted, so that the effect of each model could be compared with the same geometrical contraction ratio. The aerodynamic performances of inlets were determined based on the total pressure efficiency and the mass capture ratio at the geometrical throat. Also, flow visualizations were carried out to examine the flow structure, especially around the strut. Some of the results were compared with previously examined nonstrut models. The additional shock waves generated by the strut created a large separation on the sidewalls and the strut wall, resulting in the reduction of the total pressure efficiency and the capture ratio. Due to this separation, the shock wave was observed to be oscillatory. Measurement of fluctuating wall pressure was also carried out, which revealed that, in some regions, the pressure signals were asynchronous on the left and right sides of the strut. It seems that a small difference of the separation bubble structure on each sidewall initiated a cascade effect of pressure imbalance around the struts.

Nomenclature

CR = contraction ratio
H = height
L = length
M = Mach number
P = pressure
W = width
X = axial direction
Y = vertical direction
Z = horizontal direction
α = sweep angle
β = bias angle
γ = ratio of specific heats (=1.4)
η = efficiency
σ = standard deviation

Subscripts

cw = cowl
in = inlet entrance
p = pressure
s = static condition
st = strut
t = stagnation condition
th = inlet geometrical throat
w = sidewall
0 = free stream

I. Introduction

IN the future, when the environment and resources in space will be essential to sustain ever-growing human activities, reusable launch vehicles will play a pivotal role in space development. For a manned transporter to earth orbit, horizontal takeoff is much more comfortable and enhances the possibility of commercial flight. Vehicles for such purposes require efficient and moderate acceleration to hypersonic speed in the earth's atmosphere, and thus the concept of a hypersonic airbreathing engine has been introduced. Its well-known benefit is that the vehicle need not carry a heavy oxidizer, in contrast to present-day rockets, because it "breathes" the air and uses it to burn hydrogen. Among the various types of such air-breathing engines, the scramjet engine seems to be the most promising in the hypersonic flight range. In Japan, both experimental and computational analysis of scramjet components has been performed in the National Aerospace Laboratory (now a part of the Japan Aerospace Exploration Agency) for several years,[1–10] including sub scale engine tests in the Ramjet Test Facility since 1994.[11–13] To realize a practical engine, however, many problems remain to be solved, one of which is the efficient and stable compression of hypersonic incoming air. In principle, a scramjet engine utilizes shock waves, which cannot be avoided in the supersonic flow field, to compress the air sufficiently for combustion. One engine configuration, originally proposed by NASA Langley Research Center,[14] is a "sidewall compression-type" inlet. Its principal advantages are that the geometry is quite simple and that a spilled flow (spillage) due to an open bottom enables the engine to operate in a rather lower range of Mach number without any geometrical modifications. This type of inlet has been investigated in several countries.[15–17] Some studies have focused on low-Mach-number regions around Mach 4 to certify its starting capabilities and aerodynamic performance.[18] The results showed reasonable aerodynamic performance as a hypersonic diffuser.

From a practical point of view, a strut or several struts located between the sidewalls are thought to be required for efficient mixing of the fuel with the airstream. Furthermore, at higher flight speed, additional compression is achieved by the strut. On the other hand, it is apparent that such an obstacle in the main stream would cause loss of total pressure and introduce another complexity into the flowfield. However, its effects on the flow structure have not been further explored. To the authors' knowledge, there have been some attempts to evaluate strut effects quantitatively.[19]

To investigate the effect of the strut on a flow field, a single strut was added to a previously tested nonstrut inlet model.[1,2] Each strut had the same thickness, whereas the length from the leading edge to geometrical throat was varied. The cowl length, from its leading edge to the geometrical throat, was the other parameter of the experiments, and four different geometries were examined. The

Presented as Paper 1993-0741 at the 31st Aerospace Sciences Meeting & Exhibit, Reno, NV, 11–14 January 1993; received 20 May 2005; revision received 29 August 2005; accepted for publication 19 November 2005. Copyright © 2006 by the Japan Aerospace Exploration Agency. Published by the American Institute of Aeronautics and Astronautics, Inc., with permission. Copies of this paper may be made for personal or internal use, on condition that the copier pay the $10.00 per-copy fee to the Copyright Clearance Center, Inc., 222 Rosewood Drive, Danvers, MA 01923; include the code 0748-4658/06 $10.00 in correspondence with the CCC.

*Subgroup Leader, Engine System Subgroup, Combined Propulsion Research Group, 1 Kimigaya Koganezawa. Member AIAA.

†Group Leader, Combined Propulsion Research Group, 1 Kimigaya Koganezawa. Member AIAA.

‡Senior Researcher, Engine System Subgroup, Combined Propulsion Research Group, 1 Kimigaya Koganezawa.

aerodynamic losses and pressure distributions were measured and compared with those of nonstrut models. Also, visualization by the schlieren method was carried out. These observations revealed the existence of shock wave–boundary layer interaction near the throat region.

Because the flow is divided by the strut, there is a good chance that the flow on the left and that on the right side of the strut have different physical properties. This would lead to an asymmetric flow structure, such as boundary layer separation, and enhance the asymmetry in both a steady and an unsteady manner. Thus, the constant load on the strut due to the asymmetric pressure field must be considered in actual design.

In addition to the flow visualization, the unsteady pressure at symmetric locations on the left and right sides of the strut was measured with flash-mounted sensors. The ensemble average and standard deviation of the pressure signals were evaluated on both sides of the strut and the differences were examined. Also, the correlation of the signals measured at the symmetric locations was evaluated to clarify the asymmetric motion of the unsteady flowfield.

II. Experimental Apparatus and Models

A. Wind Tunnel and Measurement Devices

All experiments were conducted in a Mach 4 blowdown-type wind tunnel[2] with a 100 by 110-mm rectangular test section, as shown in Fig. 1. The freestream Mach number was 4.06 ± 0.005. The total pressure, P_{t0}, was about 1.66 MPa for the steady measurements and 2.16 MPa for the unsteady measurements. The variance of the total pressure during an experiment was within 50 kPa. The total temperature was room temperature. The duration of the blowdown was about 30 s, and pressure at up to 14 ports on the sidewall and strut wall was measured by a multiplex scanning device (Scanivalve®) with a 50-psi (350-kPa)-range pressure transducer. The pitot pressures at the throat section were also measured with Scanivalve with a 100-psi (700-kPa) transducer. Each port was scanned at 0.5-s intervals and about 10 samples were recorded. For the fluctuating pressure measurements, small transducers (Kulite® XCQ062 series) were flush-mounted on the top wall of the model. This transducer has a diameter of 1/16 in. (1.6 mm) and its maximum range was 50/100 psi (350/700 kPa). Because of the perforated screen that protects the diaphragm from dust particles, the bandwidth of these transducers is about 50 kHz. Because the protrusion of the sensor into the stream causes an increase of fluctuating signals, the flushness of the transducers was carefully checked by visual inspection and a "razor edge" detection method, the edge of a razor being slid across the surface of the wall to detect any "bumps" due to the protrusion of the transducer. The signals were digitized in 12 bits and recorded by a wave analyzer (Yokogawa® AR4400). Actual data processing was carried out using a Linux-base personal computer after the data were transferred from the analyzer via a GP-IB connection. Prior to the experiments, the measurement system was calibrated, and its end-to-end uncertainty was confirmed to be less than 0.5%.

The wall boundary layer of the wind tunnel was measured with a pitot rake. Its 99%-velocity thickness was about 10 mm at the inlet entrance. The unit Reynolds number was 7×10^7 m^{-1}. Considering the velocity profile and Reynolds number, the incoming flow and the boundary layer were fully turbulent.

Both sides of the test section hold Pyrex™ glass windows so that optical visualizations such as the schlieren method could be carried out.

B. Inlet Models

Figure 2 is an illustration of a typical inlet model. It consisted of a pair of sidewalls, a single strut, and a cowl. The leading edges of both the sidewalls and the strut had the same sweep angle, α, of 45 deg. The models were attached directly to the top or side surface of the wind tunnel; thus, the inlet swallowed the boundary layer that developed on the tunnel wall. Because the shock wave inside the inlet initially emanated from the leading edge of the sidewall, in a two-dimensional sense, it was assumed that all the consequent shock wave planes were parallel to the leading edge. Thus, the density jump due to the shock waves could be perceived most sensitively by observation inside the inlet parallel to the leading edge with the schlieren method. The models were placed on the glass side surface of the wind tunnel, and the light path was set parallel to the leading edge of the inlet sidewall, as shown in Fig. 1 (Location B). The height of the models, H, was 35 mm, about three times as high as the incoming boundary layer thickness. The entrance area, $H \times W_{in}$, and the distance between the leading edge and the throat (110 mm) were the same as those of the previously tested nonstrut models.[1,2]

The shape of the sidewall and the thickness of the strut were fixed, resulting in a fixed geometrical contraction ratio (CR) of 5. The leading edge angle of the sidewall was 4.8 deg, resulting in a CR of 3 without the strut. The experimental parameters were the strut and cowl length between their leading edges and the model's geometrical throat. By varying the length of the strut (denoted as L_{st} in Fig. 3), the tip angle of the leading edge changed, as illustrated in Fig. 3. As for the cowl, the tip angle was constant whereas L_{cw} was variable, also as shown in Fig. 3. Five struts and four cowls were prepared, a total of 20 different combinations. See Table 1 for a summary of the parameters. Struts and cowls were designated using L_{st} and L_{cw} values, such as "STRUT-10" or "COWL-0" (numbers are in mm; see Fig. 3). Seven pressure holes were tapped on both the sidewall and the strut wall along the line located 1 mm upstream of the throat line. Pitot pressures over the throat area were measured at the same

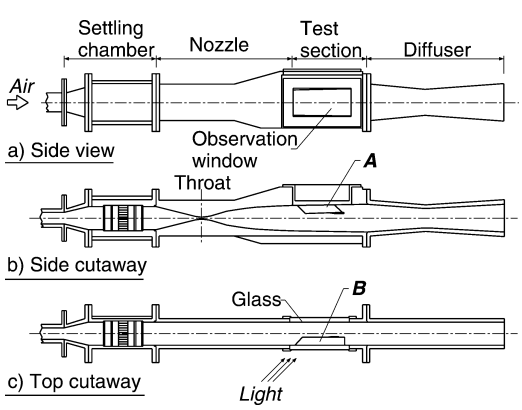

Fig. 1 Wind tunnel.

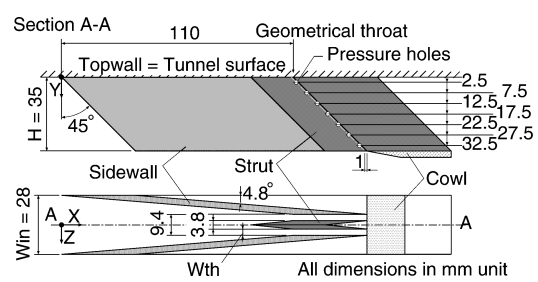

Fig. 2 Schematic view of model.

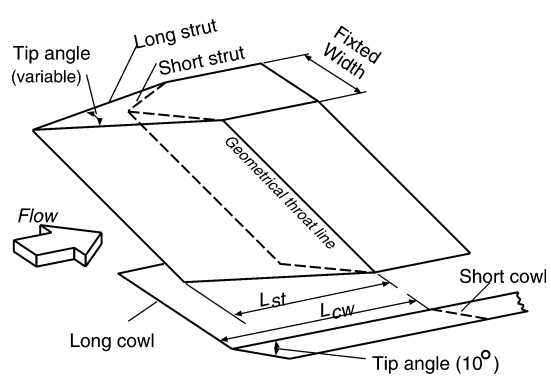

Fig. 3 Strut/cowl configuration.

Table 1 Geometrical parameters

Name	STRUT-10	STRUT-15	STRUT-20	STRUT-25	STRUT-30
L_{st}	10 mm	15 mm	20 mm	25 mm	30 mm
Tip angle	21.5 deg	14.4 deg	10.9 deg	8.7 deg	7.2 deg
Name	COWL-0	COWL-10	COWL-15	COWL-20	
L_{cw}	0 mm	10 mm	15 mm	20 mm	
Tip angle		10 deg (fixed)			

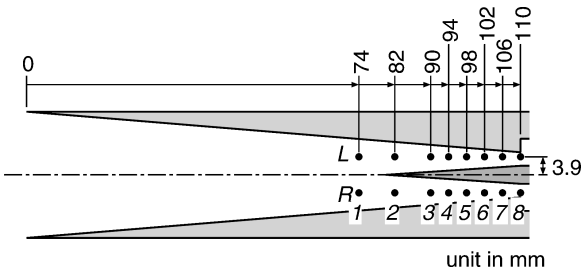

Fig. 4 Kulite sensor locations.

height as that the wall pressures were measured. For evaluation of the total pressure and other aerodynamic values, the static pressure at the point of pitot pressure measurement is required. Here, the static pressure at z was linearly interpolated from the sidewall and strut wall pressures, as follows:

$$P_s = P_w + (P_{st} - P_w)/W_{th} \times (z_w - z) \tag{1}$$

Here, z_w denotes the position of the sidewall, and z varies from z_{st}, the location of the strut wall, to z_w. Two extreme evaluations in which P_s was solely replaced by P_{st} or P_w were also carried out. The variance of the averaged total pressure and mass capture ratio from the current interpolated method were both within 3%. Note that with STRUT-10, the variance of the total pressure was as large as 9%. With the uncertainty of the position of the measurements and the pressure measuring device, overall uncertainty of the averaged total pressure and the mass capture ratio were 7% (13% for STRUT-10) and 6%, respectively.

For the fluctuating pressure measurement, Kulite sensors were flash-mounted on the top wall around the strut area. Eight symmetric locations on the left and right sides of the strut, 3.9 mm from the centerline, were selected as shown in Fig. 4. Here, each sensor location is denoted by side and number from upstream to downstream, for example, "L-7."

Note that due to limitation in the number of sensors, only some of the positions were simultaneously measured in a run.

Prior to each experiment, the model dimensions were mechanically measured with calipers and a depth gauge. The variance of W_{in} was 27.7 ± 0.2 mm, whereas that of W_{th} was 3.0 ± 0.05 mm on both the left and right sides. The maximum difference of the right and left side throat width was 0.03 mm.

III. Results and Discussion

A. Schlieren Observation

The schlieren photos of Fig. 5, which was taken with exposure time 1/60 s, show the shock wave patterns inside the inlet with each strut. Because the view line was parallel to the sidewall leading edge, the image aspect ratio was different from the actual size. To observe the whole region from the entrance to the throat, only COWL-0 was employed. They all indicated complicated shock–shock and shock–boundary layer interactions occurring around the strut region. The shock waves near the throat were not so clear because of its skewed three-dimensional structure and the oscillatory movements. The boundary layer separation of the sidewall, created by the shock wave emanating from the strut leading edge, could be observed in each picture. In the short strut case, the separation region length became compatible to that of the strut. Typically in the case of

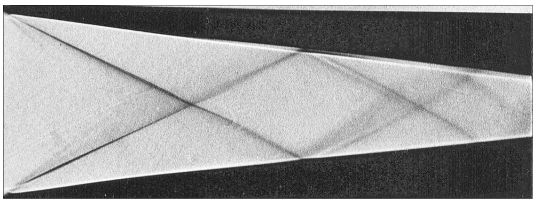

a) NON-STRUT

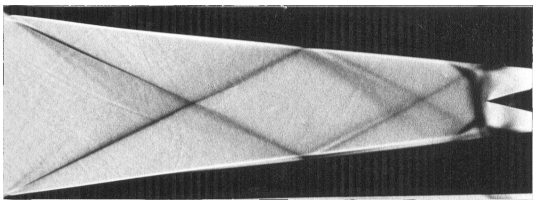

b) STRUT-10

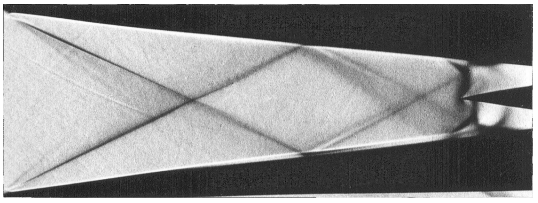

c) STRUT-15

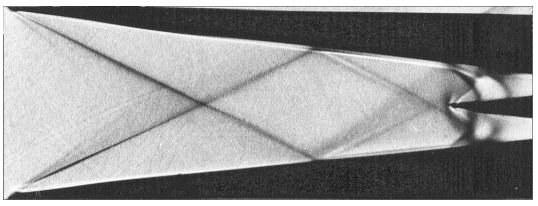

d) STRUT-20

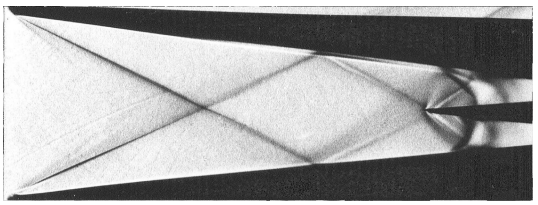

e) STRUT-25

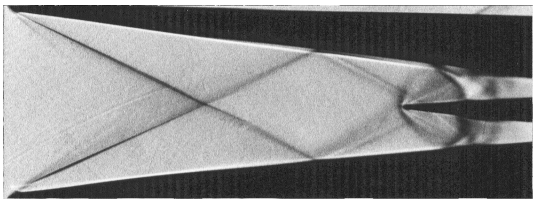

f) STRUT-30

Fig. 5 Schlieren photographs inside the model.

STRUT-10, the separation region began in roughly the same streamwise location as the strut leading edge and its end even reached the geometrical throat. However, the separation point always remained in the vicinity of the strut region, indicating that the boundary layer on the sidewall was turbulent. In some of the pictures, the location of shock waves on both sides of the strut showed an asymmetric configuration. This asymmetry was also found as the oscillation of the shock waves by observation using a high-speed video camera (Kodak EktaPro EM 1012). Figure 6 shows some examples of this oscillation. Pictures were taken at intervals of 1/1000 second. The movement of separation on the sidewall and the related shock wave (denoted as SS1 and SS2) oscillation were confirmed to be asymmetric.

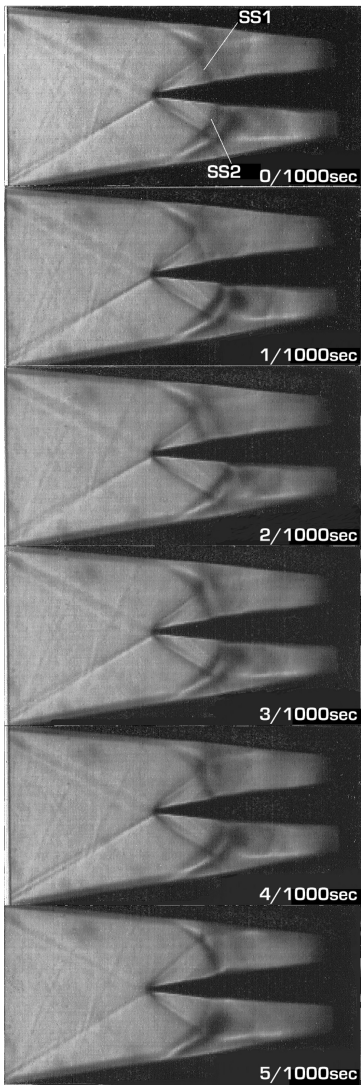

Fig. 6 Schlieren photographs of asymmetric shock motion (strut-25).

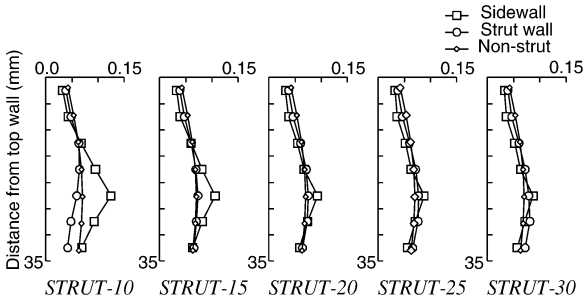

Fig. 7 Pressure distributions on the throat line.

B. Throat Wall Pressure

To distinguish the effect of strut length, the wall pressure distributions on both the sidewall and the strut wall (P_w and P_{st}, nondimensionalized by P_{t0}) are compared with COWL-0 in Fig. 7. With COWL-0, the shock wave emanated from the leading edge of the cowl located downstream of the throat, so it is assumed that the cowl shock had no effect on the distribution of wall pressures at the throat. In Fig. 7, the sidewall pressure distribution of the nonstrut model with the same α and CR is also indicated. In every case, P_{st} showed distributions similar to those of P_w of the nonstrut model. On the other hand, P_w distributions showed some differences, depending on the length of struts. When the strut was short, a high-pressure region appeared, which diminished as the strut became longer, at midheight. The struts created shock waves which were reflected on the sidewall and caused separation, as was mentioned in the previous section. Passing over this separation bubble, the air was initially

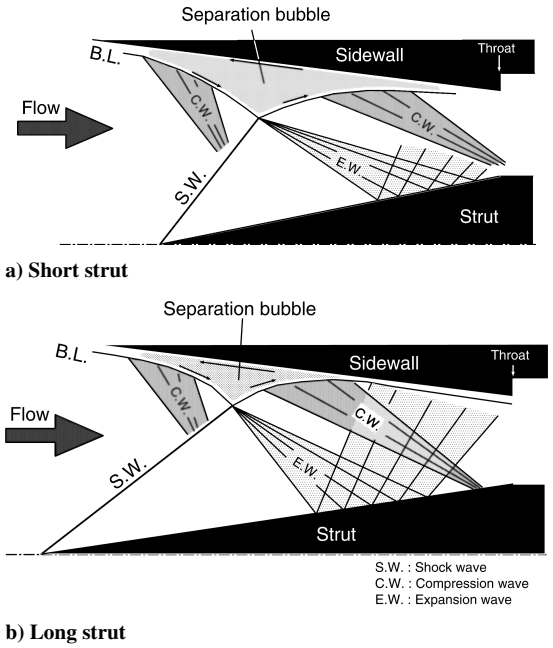

Fig. 8 Wave structure around strut.

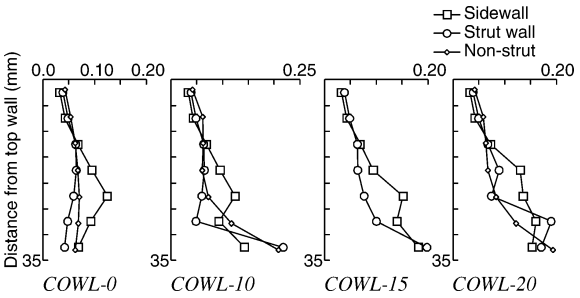

Fig. 9 Pressure distributions on the throat line.

compressed, then expanded and finally compressed again. This wave system for the short strut and the long one are illustrated and compared in Fig. 8. In the case of the short strut, the bubble length was almost the same as that of the strut. Thus, the final compression wave could not reach upstream of the strut throat line and the reflected expansion wave could not reach upstream of the sidewall throat line. As a result, the pressure value on the strut was a little lower. When the strut became longer (i.e., the leading-edge angle of the strut became smaller), the pressure rise due to the shock wave created by the strut became smaller and thus a smaller bubble was created. The flow near the strut surface passed through all the waves which emanated from the bubble, and these waves, which were reflected on the strut, traveled back on the sidewall well upstream of the throat line. Thus, the pressures on both walls became similar and lower.

Nonuniform pressure distribution along the throat line was formed as follows. Due to the swept-back angle, shock waves from the sidewalls and strut have a structure analogous to that created around a rhombic delta wing.[20] In the current geometry, the shock waves had a two-dimensional plane shape at midheight of the models, but curved near the top wall. There, the refraction angle of the flow due to the shock wave became smaller, as did the pressure rise. As for the region near the cowl, the wall pressure also decreased. This is one of the prominent effects of the open bottom configuration. Because of the difference of the pressure inside and outside the inlet, an expansion region was created over the bottom plane of the inlet, and this expansion diminished the wall pressure near the cowl.

In Fig. 9, the cowl length effects in the STRUT-10 case are also characterized in the form of the wall pressure distributions at the throat. The shock wave that was generated at the leading edge of the cowl created a high-pressure region near the cowl on both the sidewall and the strut wall. Again, P_{st} distributions were similar to that of the nonstrut inlet with the same cowl lengths. In the COWL-10

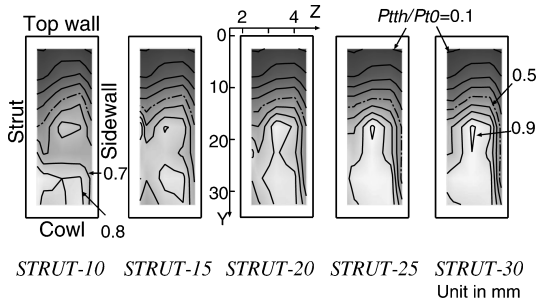

Fig. 10 Total pressure distributions at throat.

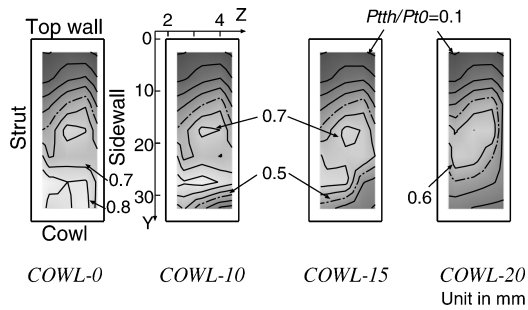

Fig. 11 Total pressure distributions at throat.

case, P_{st} near the cowl increased to a level about four times as high as that of the COWL-0 case. When the cowl became longer, this high-pressure region gradually widened toward the top wall, and in case of COWL-20, about half of the throat region was affected.

C. Total Pressure Distribution at the Throat

In Fig. 10, distributions of nondimensionalized total pressure at the throat ($P_{t\mathrm{th}}/P_{t0}$) are compared for the various struts, with the same COWL-0. The effect of the sidewall boundary layer separation can also be seen in these contours. From the top wall to the line which indicates a value of 0.4, no significant differences could be observed. Below this region, the separation bubble on the sidewall affected the stream, reducing the value and distorting the distribution. The high-total pressure region was located in the lower half of the flow passage in the case of STRUT-30. As the strut became shorter, this region was divided into two segments, one of them remaining at the midpoint of the stream, the other being pushed away to the cowl side.

With varying cowl length, the total pressure distributions with STRUT-10 are compared in Fig. 11. The effect of cowl length seemed to appear first at the corner of the side wall and the cowl. The low-total-pressure region (in this case, say, below 0.5) spread out from the corner. This tendency was the same as that in the case of longer struts (not shown here). One of the reasons for this was the thicker boundary layer on the sidewall compared with that of the strut wall, resulting in the formation of a larger separation region.

D. Total Pressure Efficiency and Capture Ratio

The total pressure efficiency, η_{PT}, and the capture ratio for all the cases examined are shown in Fig. 12. The quantity η_{PT} was the average value of the local $P_{t\mathrm{th}}/P_{t0}$, weighted by the geometrical area. The capture ratio was defined as the throat mass flux normalized by the entrance mass flux. In Fig. 12, the data of nonstrut models with the same α and CR are also indicated. In general, η_{PT} became higher as the length of the strut became longer. In the case of STRUT-30, η_{PT} did not show notable change with varying cowl length, whereas in the case of STRUT-10, η_{PT} apparently became higher with a shorter cowl. With long cowl and short strut, the boundary layer on the inner surface of the cowl separated due to the shock wave created by the strut with a large leading-edge angle, increasing the loss of total pressure severely. As for the long-strut case, the shock wave from the strut became weaker and so the separation on the inner surface of the cowl was not so significant. Thus, P_t was somewhat higher.

The value of the capture ratio was determined by the spillage, which is affected by the structure of the shock waves and by the

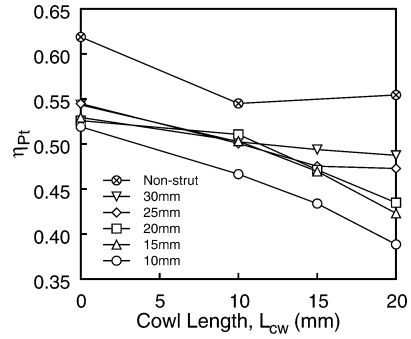

a) Total pressure recovery

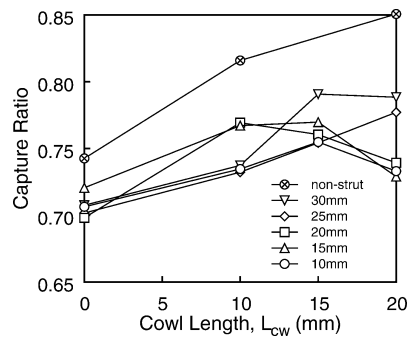

b) Capture ratio

Fig. 12 Total pressure efficiency and mass capture ratio.

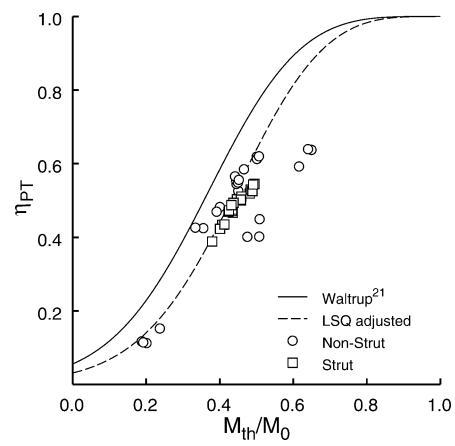

Fig. 13 Correlation of η_{PT} and $M_{\mathrm{th}}/M_{\mathrm{in}}$.

position of the cowl which prevents the flow from going outward from the inlet. The outgoing flow direction around the strut became considerably steep, since there was an additional series of shock waves in that region. Thus, the extension of the cowl had the potential to increase the capture ratio drastically. With STRUT-10, however, the capture ratio did not differ so much when L_{cw} was greater than 10 mm. In this case, the leading edge of the strut was located downstream of the leading edge of the cowl. Thus, the additional spillage which would be created by a strut-originated shock wave did not exist. Moreover, further extension of the cowl (typically, with COWL-20) caused a decrease of the capture ratio. This effect cannot be explained clearly. With long struts, for example, STRUT-25 or -30, extension of the cowl resulted in linear effects, increasing the capture ratio notably.

In any case, the capture ratio was about 2 to 12% smaller than that of the nonstrut model with the same cowl geometry, and η_{PT} was indicated to have about a 3 to 17% lower value than the nonstrut models. These aerodynamic losses were significant with the "short strut, long cowl" configuration.

Figure 13 shows the correlation between η_{PT} and the ratio of the throat Mach number and the free stream Mach number (M_{th}/M_0). The quantity M_{th} was the average value, weighted by the local area

at the measuring point. The squares represent the results of the strut models and the circles denote the data obtained with the nonstrut models with various α and CR.[1] The results of the nonstrut models were scattered because the static pressure at the throat was extrapolated from the P_w of one sidewall. Thus, it contained considerable error. In the case of the strut models, the static pressure was interpolated as was mentioned earlier, and as a result, this method gave a fairly good estimation of the static pressure distribution. In Fig. 13, the empirical correlation introduced by Waltrup et al.[21] is also indicated. Waltrup's equation represents the kinetic energy efficiency, η_{KE}, and η_{KE} is transformed into the total pressure efficiency, η_{PT}, along with the equation

$$\eta_{\mathrm{KE}} = 1 - 0.4[1 - (M_{\mathrm{th}}/M_0)]^4 \tag{2}$$

$$\eta_{\mathrm{PT}} = \left[1 + (\gamma - 1/2)M_0^2(1 - \eta_{\mathrm{KE}})\right]^{\gamma/(1-\gamma)} \tag{3}$$

Using Eq. (3), the current experimental η_{PT} could be transformed into η_{KE}. Assuming that η_{KE} could be estimated as a form similar to that of Waltrup's, the least-squares method was applied and the empirical equation for the present data was obtained as follows:

$$\eta_{\mathrm{KE}} = 1 - 0.528[1 - (M_{\mathrm{th}}/M_0)]^{3.63} \tag{4}$$

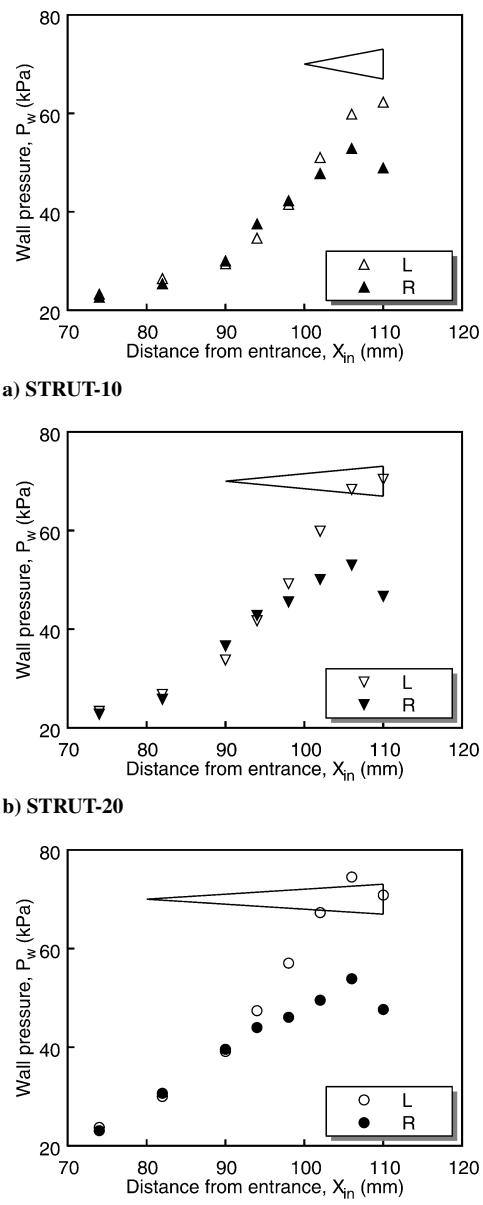

a) STRUT-10

b) STRUT-20

c) STRUT-30

Fig. 14 Time-averaged pressure.

The dashed curve in Fig. 13 shows the retransformed η_{PT} calculated by Eq. (4). One of the reasons for the shift from Waltrup's curve was the thick incoming boundary layer.

E. Unsteady Pressure Measurement

Figure 14 shows time-averaged pressure distributions measured with STRUT-10, -20, and -30. Apparent pressure differences were observed at L/R-7 and at L/R-8 with STRUT-10 and at L/R-4 and its downstream locations with STRUT-30. The factor of the difference of the maximum pressure that was observed at L/R-7 was about 1.3 for the STRUT-10 and -15 models and 1.5 for the STRUT-20, -25, and -30 models, revealing the existence of a constant load on the strut, at least near the top wall region. By comparing the results with the schlieren photographs, a pressure difference was initiated in the separation region on the sidewall, indicating that the size and structure of the separations on the left and right sidewalls were different. Note that a sudden expansion occurred at the throat due to the enlargement of the flow passage. Thus, the P_w at L/R-8 somehow showed a value lower than that obtained at L/R-7.

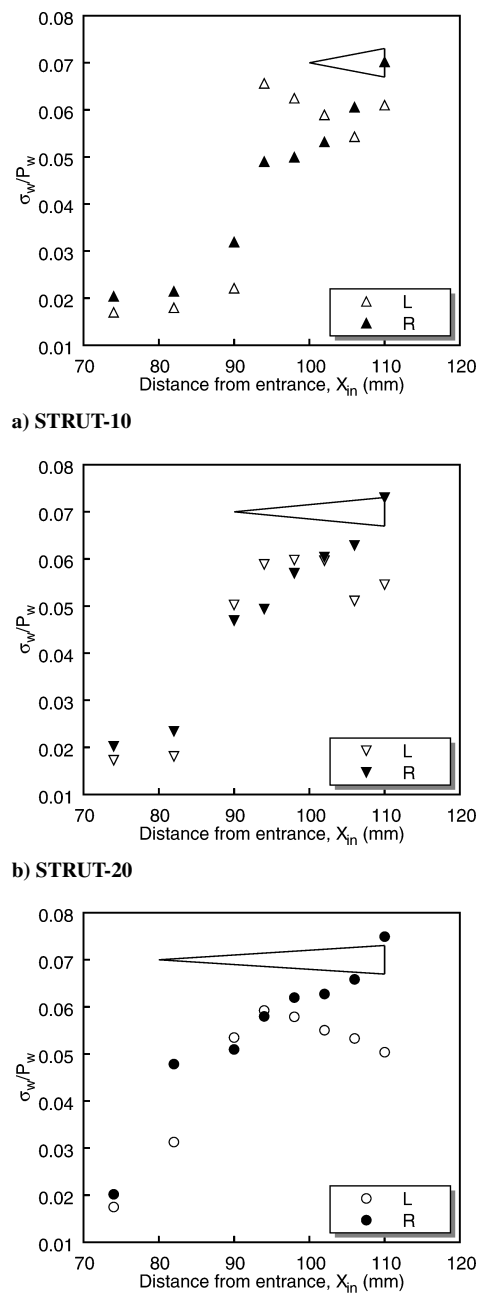

a) STRUT-10

b) STRUT-20

c) STRUT-30

Fig. 15 Normalized standard deviation.

In Fig. 15, the normalized standard deviations (σ_p/P_w) are compared for the left and right sides of the strut. With STRUT-10, σ_p/P_w jumped upstream of the strut and showed discrepancies on the left and right sides. With STRUT-30, σ_p/P_w increased at the leading edge of the strut, and the discrepancy was rather big at that point. However, σ_p/P_w became almost identical just downstream of the leading edge (L/R-3, 4), and the discrepancies once again became greater at the midpoint of the cord of the strut and downstream. A larger standard deviation usually occurs in the shock wave and boundary layer interaction region where a shock wave oscillates.[22] The location where σ_p/P_w increased again corresponds to the point where large separation and an associated shock wave on the sidewall were observed in the schlieren photos. Since σ_p is the integral of the power spectrum density, the difference of σ_p on the left and right sides could be interpreted to mean that the magnitude of the oscillation was asymmetric.

In order to examine the unsteady asymmetries of the pressure, the cross-correlations on the left and right sides of the strut were evaluated and are shown in Fig. 16. The pressure signals at two symmetric points, such as L-1 and R-1, are depicted as a pair. As for the short strut (STRUT-10), a strong correlation was observed at L/R-4 at $\tau = 0$ ms. Also, at L/R-3 and L/R-5, weak peaks were observed. Although the average values and the standard deviations were different on the left and right sides, as was previously mentioned, at least the motion of the shock wave was synchronous. On the other hand, with STRUT-30, L/R-2 to L/R-4 signals had weak peaks at $\tau = 0.05$ ms. Although their average values and standard deviations were almost identical, the motion of the shock wave was asynchronous. The same sort of asynchronous results were observed with every strut other than STRUT-10. From this observation, it is deduced that the asynchronous motion and asymmetry of the two flow fields on the left and right sides of the strut were two independent phenomena.

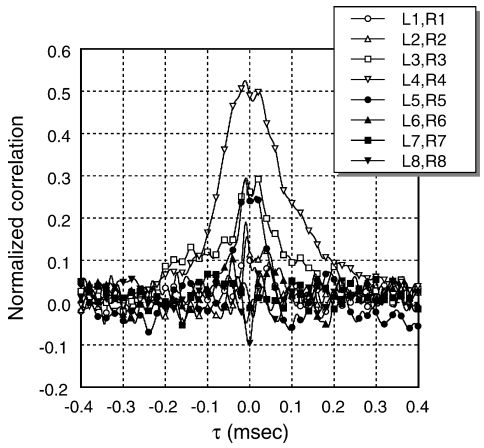

a) STRUT-10

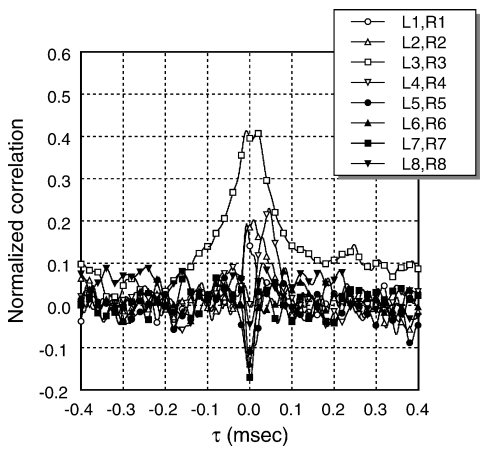

b) STRUT-20

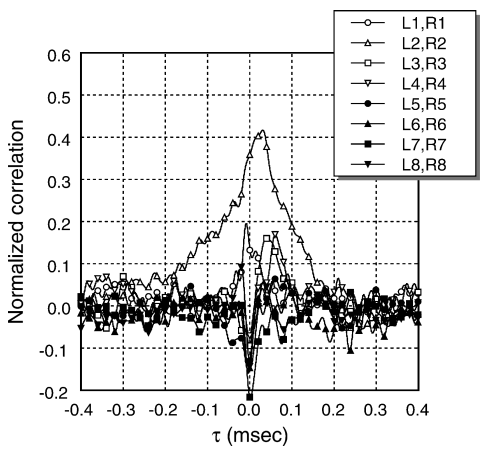

c) STRUT-30

Fig. 16 Normalized standard deviation.

IV. Conclusions

The roles of the strut in the scramjet comprise enhancement of fuel mixing and additional compression in a restricted overall length. However, the configuration of the strut must be considered very carefully, because it creates asymmetric separation problems and thus flow distortion. The present parametric study of the lengths of struts and cowls led to the following conclusions.

1) The schlieren photographs clarified the existence of large separation bubbles in the strut area. Oscillation of the shock wave induced by the separation was also confirmed by high-speed video observation.

2) A short strut caused high local pressure in the throat region and pressure distortion between the sidewall and the strut.

3) Longer and lower leading-edge angle struts did not create high local pressure, and the distribution of the wall pressure along the throat line was similar to that of the nonstrut model with the same swept-back angle and contraction ratio.

4) The η_{PT} of the strut models was 3 to 17% less than that of the nonstrut model with the same swept-back angle and contraction ratio. The "longer strut and shorter cowl" combination yielded the highest performance.

5) The capture ratio of the strut models was 2 to 15% less than that of the nonstrut model. The longer cowl with longer struts, but not with the short struts, showed better performance.

6) The value of η_{PT} against M_{th}/M_0 was slightly lower than predicted by Waltrup's empirical equation. The thick incoming boundary layer was one of the reasons for this lesser value.

7) The pressure on the top wall around the strut was of an asymmetric nature in both steady and unsteady manners, suggesting the existence of both static and dynamic load on the strut.

References

[1]Tani, K., Kanda, T., Komuro, T., Murakami, A., Kudo, K., Wakamatsu, Y., Masuya, G., and Chinzei, N., "Flow Measurement in Scramjet Inlet," *Proceedings of 17th International Symposium on Space Technology and Science*, ISTS Board, Tokyo, 1990, pp. 831–836.

[2]Kanda, T., Komuro, T., Masuya, G., Kudo, K., Murakami, A., Tani, K., Wakamatsu, Y., and Chinzei, N., "Mach 4 Testing of Scramjet Inlet Models," *Journal of Propulsion and Power*, Vol. 7, No. 2, 1991, pp. 275–280.

[3]Ishiguro, T., Ogawa, S., and Wada, W., "Numerical Calculation of Scramjet Inlet Flow," NAL Technical Rept., TR-1174T, 1992.

[4]Mitani, T., Ueda, S., Tani, K., Sato, S., Miayjima, H., Matsumoto, M., and Yasu, S., "Validation Studies of Scramjet Nozzle Performance," *Journal of Propulsion and Power*, Vol. 9, No. 5, 1993, pp. 725–730.

[5]Masuya, G., Komuro, T., Murakami, A., Shinozaki, N., Nakamura, A., Murayama, M., and Ohwaki, K., "Ignition and Combustion Performance of Scramjet Combustors with Fuel Injection Struts," *Journal of Propulsion and Power*, Vol. 11, No. 2, 1995, pp. 301–307.

[6]Saito, T., Wakamatsu, Y., Mitani, T., Chinzei, N., Shimura, T., and Kanda, T., "Mach 8 Testing of a Scramjet Engine Model," *Proceedings of the 11th International Symposium on Space Technology and Science*, Vol. 1, ISTS Publication Comm., ISTS96-a-2-11, 1996, pp. 58–63.

[7]Sunami, T., Sakuranaka, N., Tani, K., Hiraiwa, T., and Shimura, T., "Mach 4 Tests of a Scramjet Engine–Effects of Isolator," *Proceedings of the 13th International Symposium on Airbreathing Engines*, AIAA, Reston, VA, 1997, pp. 615–625.

[8]Kanda, T., Hiraiwa, T., Mitani, T., and Tomioka, S., "Mach 6 Testing of a Scramjet Engine Model," *Journal of Propulsion and Power*, Vol. 13, No. 4, 1997, pp. 543–551.

[9]Kanda, T., Wakamatsu, Y., Ono, F., Kudo, K., Murakami, A., and Izumikawa, M., "Mach 8 Testing of Scramjet Engine Models," AIAA Paper 99-0617, Jan. 1999.

[10]Kanda, T., Wakamatsu, Y., Sakuranaka, N., Izumikawa, M., Ono, F., and Murakami, A., "Mach 8 Testing of a Scramjet Engine with Ramp Compression," AIAA Paper 2000-0616, Jan. 2000.

[11]Yatsuyanagi, N., Chinzei, N., and Miki, Y., "Initial Test of a Sub-Scale Scramjet Engine," *Proceedings of the 12th International Symposium on Airbreathing Engines*, Melbourne, Australia, Vol. 2, AIAA, Washington, DC, 1995, pp. 1330–1337.

[12]Yatsuyanagi, N., Chinzei, N., Mitani, T., Wakamatsu, Y., Masuya, G., Iwagami, S., Endo, M., and Hanus, G., "Ramjet Engine Test Facility (RJTF) in NAL-KRC, Japan," AIAA Paper 98-1511, April 1998.

[13]Chinzei, N., "Scramjet Engine Tests at NAL-KPL, Japan," ISABE-2003-1171, Cleveland, OH, Aug. 2003.

[14]Trexler, C. A., and Souder, S. W., "Design and Performance at a Local Mach Number of 6 of an Inlet for an Integrated Scramjet Concept," NASA TN D-7944, 1975.

[15]Holland, S. D., and Perkins, J. H., "Contraction Ratio Effects in a Generic Three-Dimensional Sidewall Compression Scramjet Inlet : A Computational and Experimental Investigation," AIAA Paper 91-1708, June 1991.

[16]Kumar, A., Singh, D. J., and Trexler, C. A. "A Numerical Study of the Effects of Reverse Sweep on Scramjet Inlet Performance," *Journal of Propulsion and Power*, Vol. 8, No. 3, 1992, pp. 714–719.

[17]Vinogradov, V. A., and Stepanov, V. A., "Numerical and Experimental Investigation of Airframe Integrated Inlet for High Velocities," *Journal of Propulsion and Power*, Vol. 8, No. 1, 1992, pp. 151–157.

[18]Tani, K., Kanda, T., and Tokunaga, T., "Starting Characteristics of Scramjet Inlets," *Proceedings of the 11th International Symposium on Airbreathing Engines*, Vol. 2, AIAA, Washington, DC, 1993, pp. 1071–1080.

[19]Tani, K., Kanda, T., Kudo, K., Murakami, A., Komuro, T., and Itoh, K., "Aerodynamic Performance of Scramjet Inlet Models with a Single Strut," AIAA Paper 93-0741, Jan. 1993.

[20]Koide, S., Griesel, C. J. W., and Stollery, J. L., "Correlation of Shock Angles Caused by Rhombic Delta Wings," *AIAA Journal*, Vol. 34, No. 7, 1996, pp. 1529–1531.

[21]Waltrup, P. J., Billig, F. S., and Stockbridge, D., "Engine Sizing and Integration Requirements for Hypersonic Airbreathing Missile Applications," AGARD CP-307, 1982.

[22]Tani, K., and Dolling, D. S., "Fluctuating Wall Pressures in a Mach 5 Crossing Shock/Turbulent Boundary Layer Interaction Including Asymmetric Effects," AIAA Paper 96-0045, Jan. 1996.